

## Preparation and characterization of nanoparticle and nanocrystal from sago starch

<sup>1</sup>Ramli, M.E., <sup>1</sup>Zulkurnain, M., <sup>2</sup>Nazir, N. and <sup>1,\*</sup>Uthumporn, U.

<sup>1</sup>Food Technology Division, School of Industrial Technology, 11800 USM, Pulau Pinang, Malaysia

<sup>2</sup>Faculty of Agricultural Technology, Universitas Andalas, Padang, West Sumatera, Indonesia

### Article history:

Received: 5 December 2023

Received in revised form: 15 November 2024

Accepted: 26 November 2024

Available Online: 27

December 2024

### Keywords:

Sago starch,  
Pullulanase,  
Acid hydrolysis,  
Starch nanoparticle,  
Starch nanocrystal

### DOI:

[https://doi.org/10.26656/fr.2017.8\(S5\).19](https://doi.org/10.26656/fr.2017.8(S5).19)

### Abstract

There is an emerging interest in the development of starch-biomaterial for various applications such as in food emulsions. Starch has several advantages to be modified as they are low-cost material, submicron in size with a high surface area to volume ratio and abundance of functional groups for surface modifications. The objective of this study was to prepare and investigate the morphological, structural and physicochemical properties of nanoparticles (SNP) and nanocrystals (SNC) extracted from sago starch. SNP was prepared by enzymatic hydrolysis with 5% pullulanase at 58°C for 24 hrs, meanwhile SNC was produced by acid hydrolysis with aqueous sulphuric acid (H<sub>2</sub>SO<sub>4</sub>) for 5 days at 40°C. Both SNP and SNC showed a size lower than 1000 nm and a homogenous polydispersity index. The X-ray diffraction analysis showed that the relative crystallinity increased significantly ( $p < 0.05$ ) and allowed stronger hydrogen bond interaction in both SNP and SNC. Besides that, swelling power, solubility and yield of SNP were significantly higher ( $p < 0.05$ ) than SNC as it was greatly influenced by the amorphous and crystalline regions of the starch particles after hydrolysis. Moreover, SNP have a less distinct shape with a size larger than SNC favoured by self-aggregation and lower zeta potential value. Overall, SNP prepared by enzymatic hydrolysis showed the most promising materials to meet industrial demands due to the environmental friendliness (no pollution), high yield and less preparation time needed. Therefore, the newly fabricated SNP have potential as an emulsifier, encapsulating agents and others regardless of any food system.

## 1. Introduction

The science and technology of particles is a rapidly growing interdisciplinary research area by developing sustainable products using renewable and degradable materials which have special interest to the scientific industry in recent years (Feng *et al.*, 2020; Birajdar *et al.*, 2021; Zhu 2021). Starch is the second most abundant natural polymer produced in the world as a major energy source for humans and many plants (Wang *et al.*, 2015; Zhu 2018). In the family of renewable polymeric materials, starch has been demonstrated to be one of the most promising and useful materials due to its abundance, low cost, biocompatibility and biodegradability (Shariffa *et al.*, 2017). It plays important roles in the food, chemical, pharmaceutical, textile and other industries as a raw material.

Native starch granules have an onion-like ring semi-crystalline layered structure with an alternating arrangement of amorphous lamella and crystalline

lamella. It is mainly composed of two macromolecules namely amylose and amylopectin. Amylose is the main component of the amorphous region which is made up of a linear molecule of glucose units linked by  $\alpha$ -1,4-glycosidic bonds. Meanwhile, amylopectin is a branched polysaccharide composed of hundreds of  $\alpha$ -1,6-glycosidic bond chains (short linear chain), which are interlinked by  $\alpha$ -1,4-glycosidic bond linkages (Pérez and Bertoft, 2010). As a typical green biodegradable natural polymer, starch is a great candidate for producing nanocrystals (SNC) and nanoparticles (SNP).

The word 'nano' is defined as solid or colloidal particles that have at least one dimension smaller than 1000 nm (Campelo *et al.*, 2020). In parallel, nanomaterials such as starch nanoparticles and nanocrystals have attracted much attention in recent years due to the great potential for applications in composites (Ahmad, Lim, Navaranjan *et al.*, 2020), biomedicine (Nallasamy *et al.*, 2020) and food industry

\*Corresponding author.

Email: [sapina@usm.my](mailto:sapina@usm.my)

(Shao *et al.*, 2018). Due to their submicron size and high surface-to-volume ratio, SNPs and SNCs size display unique properties that differ from bulk material such as controllable release characteristics (Acevedo-Guevara *et al.*, 2018), higher solubility and bioavailability (Bhatia and Rohilla 2020) and improved delivery of several active ingredients in foods products (Fu *et al.*, 2019).

The preparation techniques of SNCs and SNPs can be classified into two different ways which are “top-down” and “bottom-up”, respectively. “Top-down” can be produced from structure and size refinement through a breakdown of larger particles. The amorphous region is less resistant to hydrogen ions and highly susceptible to acid hydrolysis compared to the crystalline structure. The amorphous part will be removed preferentially and obtain nano-scale particles with higher crystallinity known as starch nanocrystals (SNCs). However, acid hydrolysis treated with concentrated sulfuric acid or hydrochloric acid takes a long period of time (3-5 days) with low recovery yield (Velásquez-Castillo *et al.*, 2020).

In the “bottom-up” process, SNPs can be prepared from a buildup of atoms or molecules in a controlled manner. This method is promising and attractive owing to its high yield, short time and cost-effectiveness. SNPs are produced from gelatinized starch and self-assembly which native starch is pretreated with a debranched enzyme, followed by the recrystallization process (Sun *et al.*, 2014). The linear amylose of starch is produced, as a result of enzymatic hydrolysis particularly pullanase or isoamylase which re-associates during the retrogradation of starch forming a crystalline structure. The recrystallization increased the crystallinity of the nanoparticles. Since these reports, the interest in the preparation and use of SNPs has been growing steadily giving rise to simpler and more methods for SNPs production.

To the best of our knowledge, no information is currently available concerning the development of sago SNPs to address the challenges of traditional acid hydrolysis methods. Therefore, in this present work, a comparative investigation of the morphological and structural properties of SNPs and SNCs of sago starch has been compared which allows user to choose the most appropriate method for their target applications.

## 2. Materials and methods

### 2.1 Materials

The native sago starch was purchased from Tai Huat Company, Butterworth, Penang. Pullulanase (1000 NPUN/g) was supplied by Sigma-Aldrich (Castle Hill, NSW, Australia). All other chemicals were certified for

analytical grade.

### 2.2 Starch nanocrystals

Acid hydrolysis was implemented according to the method of the previous study with minor modifications (Angellier *et al.*, 2004). The preparation of starch nanocrystals (SNC) by sulfuric acid (H<sub>2</sub>SO<sub>4</sub>). Briefly, 100 g of sago starch was mixed with 250 mL of 3.16 M H<sub>2</sub>SO<sub>4</sub> for 5 days at 40°C with 160 rpm. The suspension was washed by successive centrifugations with distilled water until neutrality and then freeze-dried to obtain the SNC.

### 2.3 Starch nanoparticles

The short linear chains were obtained according to Sun *et al.* (2014) with some modifications. Briefly, 5 g of native sago starch was dispersed in 100 mL phosphate/citrate buffer solution (pH 5.0) and fully gelatinized in boiling water with vigorous stirring for 30 mins. The temperature of cooked sago starch was cooled to 58°C and 5% (v/w) of pullulanase enzyme was added. After 8 hrs of hydrolysis, the enzymatic reaction was stopped by heating at 100°C for 10 mins, and then centrifuged at 3000 rpm for 5 mins to remove the inactivated enzyme, followed by cooling to room temperature. The solutions were stored at 4°C overnight before freeze-dried for 48 hrs and the yield of SNPs was calculated.

### 2.4 Determination of amylose content

Amylose content was determined based on amylose-iodine complex formation according to the method by Abiddin *et al.* (2018). Native, SNCs and SNPs (20 mg, dry weight basis) were dissolved in 90% dimethylsulfoxide (8 mL) in 25 mL volumetric flask. The contents of the flask were vigorously agitated for 20 mins before it was heated in shaking water bath at 85°C. After 15 mins, the flask was taken out and cooled at ambient temperature. The contents of the flask were diluted with water up to 25 mL. Then, 1 mL of the diluted solution was taken out and mixed with 40 mL water and 5 mL iodine (I<sub>2</sub>) solution. The final volume was topped up to 50 mL. The solution was allowed to stand for 15 mins before the absorbance reading was taken. The absorbance was read at 600 nm by using UV-VIS spectrophotometer. The amylose content in the starch samples was determined by plotting a standard curve ( $R^2 = 0.9948$ ).

### 2.5 Particle size, zeta potential, polydispersity index

The apparent average size, polydispersity index and zeta potential of the SNC and SNP were measured by dynamic light scattering (DLS) using a Malvern

Zetasizer Nano-ZS90 (Malvern Instruments Ltd., UK). The measurement was performed using the samples prepared by dispersing the SNPs in distilled water at a concentration of 1 mg/mL and sonicated (0.3 cycles and 80% amplitude) for 2 mins before analysis.

## 2.6 X-ray diffraction pattern

The crystalline structures of the native starch and SNPs were analyzed using an X-ray diffractometer (Bruker, Rheinfelden, Germany). X-ray diffraction (XRD) was performed on an X-ray diffractometer with Cu K $\alpha_1$  radiation ( $\lambda = 0.15405$  nm) at 40 kV and 25 mA. The scanning range and rate were 4 – 40° (2 $\theta$ ) and at speed 2°/min. The relative crystallinity of SNC and SNP was determined by the ratio of the crystalline peak areas (total diffractogram areas – amorphous peak areas) to the total diffractogram area:

$$\text{Relative crystallinity (\%)} = \frac{\text{Area under the peaks}}{\text{Total area}} \times 100\%$$

## 2.7 Fourier transform infrared spectroscopy

The SNP and SNC samples were ground together with potassium bromide (KBr) and pressed into disks for scanning with a Nicolet iS10 spectrometer (Thermo Fisher Scientific Inc., Massachusetts, USA). The spectra were obtained in transmittance mode at room temperature in the air. The wavenumber range was from 4000 to 400 cm<sup>-1</sup>. The resolution was 4 cm<sup>-1</sup> and the total number of scans was 32.

## 2.8 Solubility and swelling power

The swelling power (SP) and solubility of starch samples were determined. Briefly, 2 g of samples were suspended in 100 mL of distilled water, and the suspensions were incubated at 100°C with constant stirring for 30 mins. After centrifugation at 3000 rpm for 10 mins, the supernatant was collected and dried at 105°C to constant weight, and the weights of both the dried supernatant and sediment were determined. The solubility was determined as the weight ratio of the dried supernatant to the starch. Swelling power was determined as the weight ratio of sediment in the tube to the dry starch. The solubility and swelling power were calculated as follows:

$$\text{Solubility (\%)} = \frac{\text{Dried supernatant weight}}{\text{Weight of dry starch}} \times 100\%$$

$$\text{Swelling Power} = \frac{\text{Sediment of weight (g)}}{\text{Weight of dry starch (g)}}$$

## 2.9 Scanning electron microscope

Morphology was assessed using a scanning electron microscope (Quanta FEG 650, Fei). A dried sample was placed on double-sided adhesive tape attached to a stub

and coated with gold under vacuum. The conditions of acceleration were as follows: voltage, 20Kv, and photo time, 100s. For observation, 2000 $\times$  magnification was used.

## 2.10 Statistical analysis

All data were obtained from at least duplicate experimental tests and expressed by means and standard deviations. The statistically significant level ( $p < 0.05$ ) was analyzed using one-way analysis of variance (ANOVA) followed by Tukey's post-hoc (SPSS software version 23, USA).

## 3. Results and discussion

### 3.1 Amylose content

Amylose and amylopectin are the two primary components present in starch granules (Li *et al.*, 2019). The amylose content of native and debranched sago starch is shown in Figure 1. As seen in Figure 1, the amylose content of native sago is 19.05%. The amylose content was significantly reduced in starch that underwent the acid hydrolysis process. This decrease can be attributed to the fact that the hydrolysis reaction is initiated in the amorphous region of the granule, where amylose is located and combined with the long reaction time could result in a low amylose value (Jayakody and Hoover 2002). However, after being debranched by pullulanase for 24 hrs, the amylose content of the samples was significantly increased up to 32.64%. The increase in amylose was caused by cleaving of the branching points in amylopectin and producing linear chains from starch molecules with different lengths. Similar phenomena have been observed in pullulanase debranching of tiger nut (Yan *et al.*, 2022) and lotus seed starch (Zheng *et al.*, 2020).

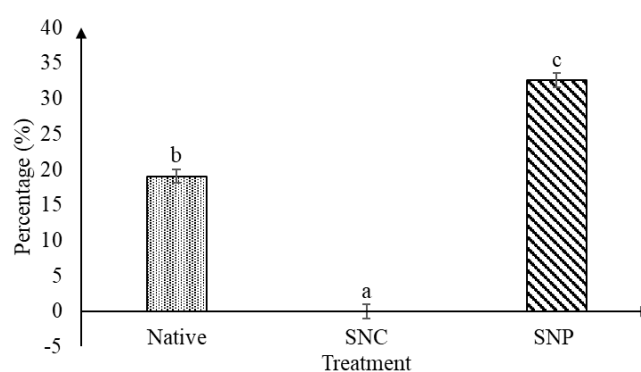


Figure 1. The amylose content of native, SNC and SNP. Data presented are mean $\pm$ SD (n = 3). Bars with different notations are statistically significantly different ( $p < 0.05$ ).

### 3.2 Particle size, polydispersity index and zeta potential

Table 1 shows the particle size, polydispersity index and zeta potential of the SNCs and SNPs fabricated from

sago starch. The Z-average value was considered the most valuable indicator for the mean size of starch, while PdI values indicated high homogeneity and stability when the PdI value was less than 0.5 (Najafi *et al.*, 2016). The acid hydrolysis had an average diameter of 214.60 nm with a mean polydispersity of 0.38, meanwhile, the SNPs size at 623.70 nm with 0.34. The higher size reduction observed for acid hydrolysis is probably associated with the extended treatment time since starch fragments are successively released from the surface of the granule resulting in a small particle size with narrow size distribution and high homogeneity of the particles.

Table 1. Particle size, polydispersity index and zeta potential of native, SNP and SNC.

Treatment	Particle Size (nm)	Polydispersity Index	Zeta Potential
SNC	214.60±3.82 <sup>a</sup>	0.38±0.03 <sup>a</sup>	-28.9±0.40 <sup>a</sup>
SNP	623.70±19.51 <sup>b</sup>	0.34±0.02 <sup>a</sup>	-18.53±0.76 <sup>a</sup>

Values are presented as mean±SD (n = 3). Values with different superscripts within the same column are statistically significantly different ( $p < 0.05$ ).

The zeta potential is a fundamental parameter which measures the strength of repulsion or attraction among the granules. Generally, the higher the absolute value of zeta potential, the more repulsive the force with respect to the DLVO classical theory. The distribution of zeta potentials of the SNC and SNP ranged from -18.53 to -28.9 mV, respectively where the dispersion more than -30 mV is relatively highly strong repulsion regardless of the particle size. It has been suggested that the hydroxyl groups in the starch molecules tend to ionize in water during acid and enzymatic hydrolysis which bears negative surface charges and zeta potential (Sadeghi *et al.*, 2017). Moreover, the higher negative charge on SNCs is contributed by the higher deprotonation of carboxyl and sulphate groups ( $\text{SO}_3^-$ ) arising from the esterification reaction of starch with sulphuric acid during the acid hydrolysis process (Wang and Copeland, 2015).

### 3.3 X-ray diffraction

X-ray diffractograms have been used to evaluate the crystalline types of starches according to diffraction angle at peak and peak intensity (Frost *et al.*, 2009). There are three X-ray diffraction patterns, depending on the organization of their amylopectin crystalline lattices in the granules, which classify into the A-, B-, or C-type. A V-type pattern also exists in starch composed of crystalline amylose inclusion complexes (Buleon *et al.*, 1998). From Figure 2, the native sago starch exhibited the C-type crystalline pattern with  $2\theta$  diffraction peaks at  $5.6^\circ$ ,  $15.0^\circ$ ,  $17.1^\circ$ ,  $17.9^\circ$  and  $23^\circ$  and a relative crystallinity of 47.3%, which was in good agreement

with previous report by Karim *et al.* (2008).

The SNCs exhibited a C-type crystallinity similar to native starch with the same diffraction peaks and had a relative crystallinity of 74.3%. The substantial increase in the relative crystallinity for SNCs is explained by the degradation of the amorphous regions of the starch granules during the acid hydrolysis treatment. However, the typical B-type XRD pattern was formed by SNP with the relative crystallinity at 51.7%. A well-defined peak at  $2\theta = 22.0^\circ$  and  $24.0^\circ$  formed when starch was subjected to gelatinization, amylopectin turns into short amylose debranching by enzyme and undergoes recrystallization. The peak  $20.0^\circ$  was assigned to a well-formed V-type XRD pattern, which is composed of amylose and naturally occurring fatty acids and phospholipids in the granules (Lalush *et al.*, 2005).

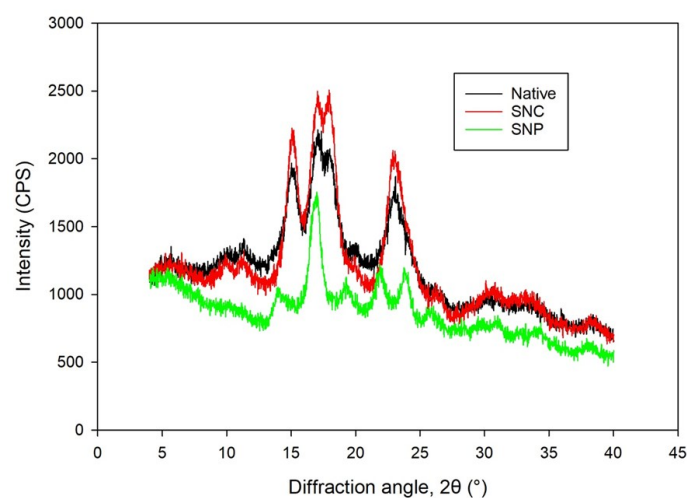


Figure 2. The XRD of native, SNC and SNP.

### 3.4 Fourier transformation infrared spectroscopy

FTIR spectroscopy can monitor the stretching, bending and deformation corresponding to the characteristics of the major functional groups. The main characteristics bands can be divided into four regions that include less than  $800\text{ cm}^{-1}$ ,  $800\text{-}1500\text{ cm}^{-1}$  (fingerprint area),  $2800\text{-}3000\text{ cm}^{-1}$  (C-H stretching vibration) and  $3000\text{-}3600\text{ cm}^{-1}$  (O-H stretching vibration) (Gutiérrez *et al.*, 2020). FTIR spectra of native, SNC and SNP are shown in Figure 3. In all spectra, broad absorption bands appeared in the range of  $3700\text{-}3000\text{ cm}^{-1}$  attributed to the stretching vibrations of the inter and intramolecular hydroxyl group (O-H) (Flores-Morales *et al.*, 2012). The characteristics band of SNC and SNP shifted to a lower wavenumber indicating the hydrogen bonds between starch particles were stronger. The absorption peak at  $2926\text{ cm}^{-1}$  can be explained by  $\text{CH}_2$  stretching vibrational modes bands associated with ring methane hydrogen atoms suggesting an amorphous regions reduction or increase in the structural organization (Zhang *et al.*, 2013). Besides that, the absorption peak that occurred at  $1640\text{ cm}^{-1}$  can be due to

the presence of bound water in starch which is in good agreement with Ahmad, Gani, Hassan *et al.* (2020) and Gutiérrez *et al.* (2020).

FTIR spectroscopy can also be used to determine the crystallinity of starch by characterizing the changes that occur in the semi-crystalline and amorphous domains within starch granules (Ahmad, Gani, Hassan *et al.*, 2020). In particular, the absorption bands at 1022 cm<sup>-1</sup> and 1047 cm<sup>-1</sup> correspond to the intensity of amorphous and ordered structures, respectively (Van Soest *et al.*, 1995). The ratio of 1047/1022 (R<sub>1047/1022</sub>) was used to quantify the internal changes in the ordered structure of starch, with the higher R<sub>1047/1022</sub> value indicating the more ordered structure. As shown in Table 2, the R<sub>1047/1022</sub> values for both SNC and SNP increased after hydrolysis, indicating enhanced short-range order structure (Miao *et al.*, 2011). This increment could be attributed to the preferential erosion of amorphous regions in SNC during acid hydrolysis and regeneration of inter-molecular association in SNP through H-bonding (Sun *et al.*, 2017; Dong *et al.*, 2022). This result was in good agreement with the XRD data (Figure 2).

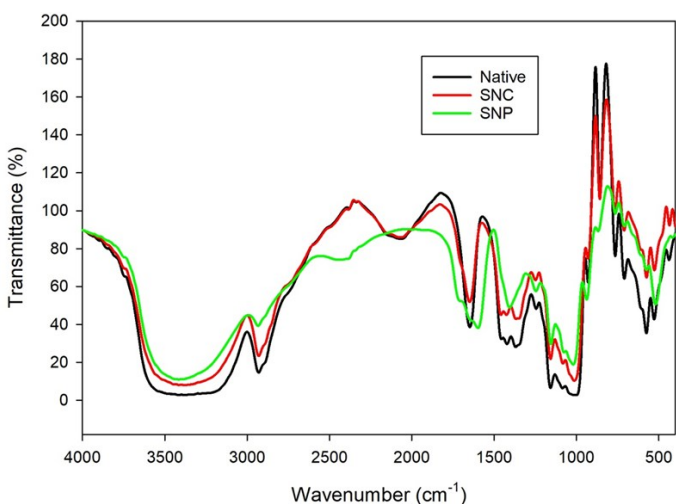


Figure 3. The FTIR of native, SNC and SNP.

Table 2. 1047/1022 ratio and relative crystallinity.

	1047/1022 ratio	Relative Crystallinity (%)
Native	1.06 <sup>a</sup>	47.3 <sup>a</sup>
SNC	1.48 <sup>c</sup>	74.3 <sup>c</sup>
SNP	1.11 <sup>b</sup>	51.7 <sup>b</sup>

Values are presented as mean±SD (n = 3). Values with different superscripts within the same column are statistically significantly different (p<0.05).

### 3.5 Morphology

The morphological properties of native, SNC and SNP were investigated. As the SEM images shown in Figure 4, native sago starch exhibited a polygonal and elliptical shape with smooth surfaces with truncated ends. Compared to the corresponding native starch, visible particle differences of SNC and SNP could be

observed. The SNC retained a clear elliptical shape with roughened surfaces, meanwhile, the SNP have a less distinct shape with a size larger than SNC. SNP are different from the native starch as the granular structure disappeared completely during gelatinization and retrogradation. The difference in shape can be attributed to the presence of hydroxyl groups which favour the interactions of hydrogen bonding and the strong tendency of particles to self-aggregate during water evaporation (Xiao *et al.*, 2016).

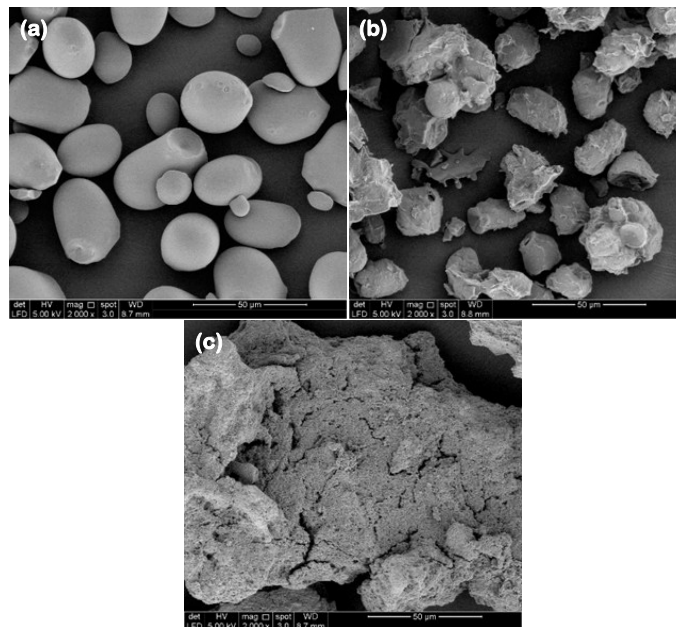


Figure 4. The morphology of a) native, b) SNC and c) SNP.

### 3.6 Swelling power and solubility

Swelling power is an assessment of the water taken up and entrapped in the gel network by hydrogen bonds during heating, cooling and stirring (Uthumporn *et al.*, 2017). Figure 5 shows that the swelling power of SNC is significantly (p<0.05) lower than SNP. During acid hydrolysis, depolymerization and disruption of the starch granules take place which causes structural reorganizations and reduces the water retention inside the granules, therefore reducing the swelling power (Martins *et al.*, 2022). Meanwhile, for SNP, starch was subjected to gelatinization and hydrolysed with pullulanase enzyme, resulting in an amorphous structure of starch granules and owing to the chance of unbound starch chains contacting with water molecule further aggravating the swelling of the starch (Ge *et al.*, 2021).

The solubility of starch refers to the ability of the amylose chain to escape from the starch granules and dissolve in water. From Figure 5, the solubility of SNC is higher compared to native starch. The hydrogen bonds of amylose and amylopectin rupture and increase the amount of available hydroxyl groups, thus increasing the solubility. However, the results showed that the solubility of SNC was significantly (p<0.05) lower

compared to SNP. The increase in amylose was caused by cleaving the branching points (1,6-glycosidic bond) in amylopectin and producing linear chains of different lengths which easily dissociate and diffuse out during swelling (Van Hung *et al.*, 2016). Thus, it increases the solubility.

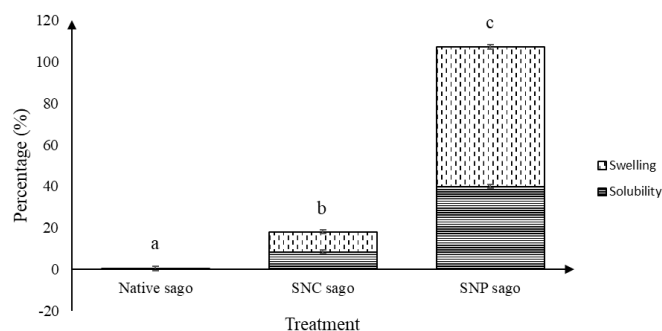


Figure 5. The swelling power and solubility of native, SNC and SNP. Data presented are mean $\pm$ SD (n = 3). Bars with different notations are statistically significantly different ( $p < 0.05$ ).

#### 4. Conclusion

In this study, we compared the properties of starch nanocrystals and starch nanoparticles extracted from sago starch through acid hydrolysis and enzymatic hydrolysis, respectively. The results demonstrated SNC and SNP produced had a particle size at 214.60 nm and 623.70 nm, respectively with higher homogeneity and zeta potential values exhibited a strong repulsion activity. The different hydrolysis approaches affected the morphologies and crystalline properties of the prepared SNC and SNP, with different starch morphology and higher crystallinity than native. Therefore, the newly developed method of SNP extracted from sago starch is hopefully to be generally safe (GRAS), green and non-toxic and can further be explored in the fields of Pickering emulsion, nutraceutical, medicine and environment.

#### Conflict of interest

The authors declare no conflict of interest.

#### Acknowledgements

Acknowledgement to Ministry of Higher Education Malaysia for Fundamental Research Grant Scheme (FRGS) with Project Code: FRGS/1/2020/STG04/USM/03/1.

#### References

Abiddin, N.Z., Yusoff, A. and Ahmad, N. (2018). Effect of octenylsuccinylation on physicochemical, thermal, morphological and stability of octenyl

succinic anhydride (OSA) modified sago starch. *Food Hydrocolloids*, 75, 138-146. <https://doi.org/10.1016/j.foodhyd.2017.09.003>

Acevedo-Guevara, L., Nieto-Suaza, L., Sanchez, L.T., Pinzon, M.I. and Villa, C.C. (2018). Development of native and modified banana starch nanoparticles as vehicles for curcumin. *International Journal of Biological Macromolecules*, 111, 498-504. <https://doi.org/10.1016/j.ijbiomac.2018.01.063>

Ahmad, A.N., Lim, S.A., Navaranjan, N., Hsu, Y.I. and Uyama, H. (2020). Green sago starch nanoparticles as reinforcing material for green composites. *Polymer*, 202, 122646. <https://doi.org/10.1016/j.polymer.2020.122646>

Ahmad, M., Gani, A., Hassan, I., Huang, Q. and Shabbir, H. (2020). Production and characterization of starch nanoparticles by mild alkali hydrolysis and ultrasonication process. *Scientific Reports*, 10, 3533. <https://doi.org/10.1038/s41598-020-60380-0>

Angellier, H., Choïnard, L., Molina-Boisseau, S., Ozil, P. and Dufresne, A. (2004). Optimization of the preparation of aqueous suspensions of waxy maize starch nanocrystals using a response surface methodology. *Biomacromolecules*, 5(4), 1545-1551. <https://doi.org/10.1021/bm049914u>

Bhatia, M. and Rohilla, S. (2020). Formulation and optimization of quinoa starch nanoparticles: Quality by design approach for solubility enhancement of piroxicam. *Saudi Pharmaceutical Journal*, 28(8), 927-935. <https://doi.org/10.1016/j.jsps.2020.06.013>

Birajdar, M.S., Joo, H., Koh, W.G. and Park, H. (2021). Natural bio-based monomers for biomedical applications: a review. *Biomaterials Research*, 25(1), 8. <https://doi.org/10.1186/s40824-021-00208-8>

Buleon, A., Colonna, P., Planchot, V. and Ball, S. (1998). Starch granules: structure and biosynthesis. *International Journal of Biological Macromolecules*, 23(2), 85-112. [https://doi.org/10.1016/S0141-8130\(98\)00040-3](https://doi.org/10.1016/S0141-8130(98)00040-3)

Campelo, P.H., Sant'Ana, A.S. and Clerici, M.T.P.S. (2020). Starch nanoparticles: production methods, structure, and properties for food applications. *Current Opinion in Food Science*, 33, 136-140. <https://doi.org/10.1016/j.cofs.2020.04.007>

Dong, H., Zhang, Q., Gao, J., Chen, L. and Vasanthan, T. (2022). Preparation and characterization of nanoparticles from cereal and pulse starches by ultrasonic-assisted dissolution and rapid nanoprecipitation. *Food Hydrocolloids*, 122, 107081. <https://doi.org/10.1016/j.foodhyd.2021.107081>

Feng, X., Dai, H., Ma, L., Fu, Y., Yu, Y., Zhou, H., Guo, T., Zhu, H., Wang, H. and Zhang, Y. (2020).

- Properties of Pickering emulsion stabilized by food-grade gelatin nanoparticles: Influence of the nanoparticles concentration. *Colloids and Surfaces B: Biointerfaces*, 196, 111294. <https://doi.org/10.1016/j.colsurfb.2020.111294>
- Flores-Morales, A., Jiménez-Estrada, M. and Mora-Escobedo, R. (2012). Determination of the structural changes by FT-IR, Raman, and CP/MAS <sup>13</sup>C NMR spectroscopy on retrograded starch of maize tortillas. *Carbohydrate Polymers*, 87(1), 61-68. <https://doi.org/10.1016/j.carbpol.2011.07.011>
- Frost, K., Kaminski, D., Kirwan, G., Lascaris, E. and Shanks, R. (2009). Crystallinity and structure of starch using wide angle X-ray scattering. *Carbohydrate Polymers*, 78(3), 543-548. <https://doi.org/10.1016/j.carbpol.2009.05.018>
- Fu, Y., Yang, J., Jiang, L., Ren, L. and Zhou, J. (2019). Encapsulation of lutein into starch nanoparticles to improve its dispersity in water and enhance stability of chemical oxidation. *Starch-Stärke*, 71(5-6), 1800248. <https://doi.org/10.1002/star.201800248>
- Ge, X., Shen, H., Su, C., Zhang, B., Zhang, Q., Jiang, H., Yuan, L., Yu, X. and Li, W. (2021). Pullulanase modification of granular sweet potato starch: Assistant effect of dielectric barrier discharge plasma on multi-scale structure, physicochemical properties. *Carbohydrate Polymers*, 272, 118481. <https://doi.org/10.1016/j.carbpol.2021.118481>
- Gutiérrez, G., Morán, D., Marefati, A., Puhagen, J., Rayner, M. and Matos, M. (2020). Synthesis of controlled size starch nanoparticles (SNPs). *Carbohydrate Polymers*, 250, 116938. <https://doi.org/10.1016/j.carbpol.2020.116938>
- Jayakody, L. and Hoover, R. (2002). The effect of lintnerization on cereal starch granules. *Food Research International*, 35(7), 665-680. [https://doi.org/10.1016/S0963-9969\(01\)00204-6](https://doi.org/10.1016/S0963-9969(01)00204-6)
- Karim, A.A., Nadiha, M.Z., Chen, F.K., Phuah, Y.P., Chui, Y.M. and Fazilah, A. (2008). Pasting and retrogradation properties of alkali-treated sago (*Metroxylon sagu*) starch. *Food Hydrocolloids*, 22 (6), 1044-1053. <https://doi.org/10.1016/j.foodhyd.2007.05.011>
- Lalush, I., Bar, H., Zakaria, I., Eichler, S. and Shimoni, E. (2005). Utilization of amylose–lipid complexes as molecular nanocapsules for conjugated linoleic acid. *Biomacromolecules*, 6(1), 121-130. <https://doi.org/10.1021/bm049644f>
- Li, L., Yuan, T.Z., Setia, R., Raja, R.B., Zhang, B. and Ai, Y. (2019). Characteristics of pea, lentil and faba bean starches isolated from air-classified flours in comparison with commercial starches. *Food Chemistry*, 276, 599-607. <https://doi.org/10.1016/j.foodchem.2018.10.064>
- Martins, P.C., Latorres, J.M. and Martins, V.G. (2022). Impact of starch nanocrystals on the physicochemical, thermal and structural characteristics of starch-based films. *LWT*, 156, 113041. <https://doi.org/10.1016/j.lwt.2021.113041>
- Miao, M., Jiang, B., Zhang, T., Jin, Z. and Mu, W. (2011). Impact of mild acid hydrolysis on structure and digestion properties of waxy maize starch. *Food Chemistry*, 126(2), 506-513. <https://doi.org/10.1016/j.foodchem.2010.11.031>
- Najafi, S.H.M., Baghaie, M. and Ashori, A. (2016). Preparation and characterization of acetylated starch nanoparticles as drug carrier: Ciprofloxacin as a model. *International Journal of Biological Macromolecules*, 87, 48-54. <https://doi.org/10.1016/j.ijbiomac.2016.02.030>
- Nallasamy, P., Ramalingam, T., Nooruddin, T., Shanmuganathan, R., Arivalagan, P. and Natarajan, S. (2020). Polyherbal drug loaded starch nanoparticles as promising drug delivery system: Antimicrobial, antibiofilm and neuroprotective studies. *Process Biochemistry*, 92, 355-364. <https://doi.org/10.1016/j.procbio.2020.01.026>
- Pérez, S. and Bertoft, E. (2010). The molecular structures of starch components and their contribution to the architecture of starch granules: A comprehensive review. *Starch-Stärke*, 62(8), 389-420. <https://doi.org/10.1002/star.201000013>
- Sadeghi, R., Daniella, Z., Uzun, S. and Kokini, J. (2017). Effects of starch composition and type of non-solvent on the formation of starch nanoparticles and improvement of curcumin stability in aqueous media. *Journal of Cereal Science*, 76, 122-130. <https://doi.org/10.1016/j.jcs.2017.05.020>
- Shao, P., Zhang, H., Niu, B. and Jin, W. (2018). Physical stabilities of taro starch nanoparticles stabilized Pickering emulsions and the potential application of encapsulated tea polyphenols. *International Journal of Biological Macromolecules*, 118, 2032-2039. <https://doi.org/10.1016/j.ijbiomac.2018.07.076>
- Shariffa, Y.N., Uthumporn, U., Karim, A.A. and Zaibunnisa, A.H. (2017). Hydrolysis of native and annealed tapioca and sweet potato starches at sub gelatinization temperature using a mixture of amyolytic enzymes. *International Food Research Journal*, 24(5), 1925-1933.
- Sun, B., Tian, Y., Wei, B., Chen, L., Bi, Y. and Jin, Z. (2017). Effect of reaction solvents on the multi-scale structure of potato starch during acid treatment. *International Journal of Biological*

- Macromolecules*, 97, 67-75. <https://doi.org/10.1016/j.ijbiomac.2017.01.003>
- Sun, Q., Li, G., Dai, L., Ji, N. and Xiong, L. (2014). Green preparation and characterisation of waxy maize starch nanoparticles through enzymolysis and recrystallisation. *Food Chemistry*, 162, 223-228. <https://doi.org/10.1016/j.foodchem.2014.04.068>
- Uthumporn, U., Nadiyah, I., Izzuddin, I., Cheng, L.H. and Aida, H. (2017). Physicochemical characteristics of non-starch polysaccharides extracted from cassava tubers. *Sains Malaysiana*, 46(2), 223-229. <https://doi.org/10.17576/jsm-2017-4602-06>
- Van Soest, J.J., Tournois, H., de Wit, D. and Vliegthart, J.F. (1995). Short-range structure in (partially) crystalline potato starch determined with attenuated total reflectance Fourier-transform IR spectroscopy. *Carbohydrate Research*, 279, 201-214. [https://doi.org/10.1016/0008-6215\(95\)00270-7](https://doi.org/10.1016/0008-6215(95)00270-7)
- Van Hung, P., Vien, N.L. and Phi, N.T.L. (2016). Resistant starch improvement of rice starches under a combination of acid and heat-moisture treatments. *Food Chemistry*, 191, 67-73. <https://doi.org/10.1016/j.foodchem.2015.02.002>
- Velásquez-Castillo, L.E., Leite, M.A., Ditchfield, C., do Amaral Sobral, P.J. and Moraes, I.C.F. (2020). Quinoa starch nanocrystals production by acid hydrolysis: kinetics and properties. *International Journal of Biological Macromolecules*, 143, 93-101. <https://doi.org/10.1016/j.ijbiomac.2019.12.011>
- Wang, S. and Copeland, L. (2015). Effect of acid hydrolysis on starch structure and functionality: a review. *Critical Reviews in Food Science and Nutrition*, 55(8), 1081-1097. <https://doi.org/10.1080/10408398.2012.684551>
- Wang, S., Wang, J., Zhang, W., Li, C., Yu, J. and Wang, S. (2015). Molecular order and functional properties of starches from three waxy wheat varieties grown in China. *Food Chemistry*, 181, 43-50. <https://doi.org/10.1016/j.foodchem.2015.02.065>
- Xiao, H., Yang, T., Lin, Q., Liu, G.Q., Zhang, L., Yu, F. and Chen, Y. (2016). Acetylated starch nanocrystals: preparation and antitumor drug delivery study. *International Journal of Biological Macromolecules*, 89, 456-464. <https://doi.org/10.1016/j.ijbiomac.2016.04.037>
- Yan, X., Diao, M., Yu, Y., Gao, F., Wang, E., Wang, Z., Zhang, T. and Zhao, P. (2022). Characterization of resistant starch nanoparticles prepared via debranching and nanoprecipitation. *Food Chemistry*, 369, 130824. <https://doi.org/10.1016/j.foodchem.2021.130824>
- Zhang, H., Tian, Y., Bai, Y., Xu, X. and Jin, Z. (2013). Structure and properties of maize starch processed with a combination of  $\alpha$ -amylase and pullulanase. *International Journal of Biological Macromolecules*, 52, 38-44. <https://doi.org/10.1016/j.ijbiomac.2012.09.030>
- Zheng, Y., Ou, Y., Zhang, Y., Zheng, B., Zeng, S. and Zeng, H. (2020). Effects of pullulanase pretreatment on the structural properties and digestibility of lotus seed starch-glycerin monostearin complexes. *Carbohydrate Polymers*, 240, 116324. <https://doi.org/10.1016/j.carbpol.2020.116324>
- Zhu, F. (2018). Relationships between amylopectin internal molecular structure and physicochemical properties of starch. *Trends in Food Science and Technology*, 78, 234-242. <https://doi.org/10.1016/j.tifs.2018.05.024>
- Zhu, F. (2021). Polysaccharide based films and coatings for food packaging: Effect of added polyphenols. *Food Chemistry*, 359, 129871. <https://doi.org/10.1016/j.foodchem.2021.129871>